Carnegie Mellon University

Annual Progress Report: 2011 Nonformula Grant

Reporting Period

July 1, 2013 – May 31, 2014

Nonformula Grant Overview

Carnegie Mellon University received $983,783 in nonformula funds for the grant award period June 1, 2012 through May 31, 2014. Accomplishments for the reporting period are described below.

Research Project: Project Title and Purpose

Automated Biomarker Identification for Cancer Detection and Prognosis – The purpose of this project is to dramatically expand the image analysis capabilities of the Omnyx digital pathology platform and to use this capacity to carry out translational research studies to further demonstrate the value of that technology for improving diagnostic and prognostic evaluation in two important patient populations. We propose to interface image analysis technology that is the intellectual property of Carnegie Mellon University with the Omnyx platform. Two research studies will be carried out, one for prostate lesions in adults and one for liver lesions in children and adults. The results of the image analysis will be compared with data on patient outcome and responsiveness to treatment.

Duration of Project

6/1/2012 – 5/31/2014

Project Overview

The goal of this project is to carry out translational research to further develop two related new cancer diagnostic methods for which proof-of-concept has been demonstrated. Carnegie Mellon University has intellectual property consisting of algorithms for (1) determining the subcellular location of marker proteins from immunohistochemistry images and identifying proteins that change subcellular location between normal and tumor tissue, and (2) robustly identifying changes in nuclear morphology that can distinguish normal from cancerous tissues in several pathologies in the liver. The research seeks to build on these results to create commercially viable diagnostic products that can be marketed by Omnyx, a pioneering digital pathology company headquartered in Pittsburgh.

The first specific aim is to perform translational research studies to determine the value of automated image analysis technology developed at Carnegie Mellon University for providing

enhanced diagnostic and prognostic information in adult prostate and pediatric/adult liver tumors. These studies will be done using paraffin-embedded tissue selected from tissue banks to cover a range of tumor grades, initial diagnoses and clinical outcome. The images will be analyzed to determine the prognostic value of the phenotypes measured by the two technologies. Additional image analysis methods will be developed as needed to improve upon the existing technologies. The second specific aim is to interface the automated technology with the Omnyx digital pathology platform and develop an appropriate and efficient clinician interface to the technology in order to facilitate the ability of the clinician to integrate its outputs into the diagnostic process.

Principal Investigator

Robert F. Murphy, PhD
Lane Professor and Head of Computational Biology
Carnegie Mellon University
5000 Forbes Avenue
Pittsburgh, PA 15213

Other Participating Researchers

Gustavo K. Rohde, PhD – employed by Carnegie Mellon University
Anil Parwani, MD; John Ozolek, MD – employed by the University of Pittsburgh
Ronald Stone, PhD; Raghavan Venugopal, MS; Michael Meissner, PhD – employed by Omnyx, Inc.

Expected Research Outcomes and Benefits

In the case of liver lesions, the development of the nuclear analysis tool may give the pathologist an ancillary and perhaps at times diagnostic tool to aid in distinguishing between differential diagnoses in liver lesions. For example, nuclear morphological features are not typically used to distinguish between nodular regenerative hyperplasia, focal nodular hyperplasia, and hepatic adenoma because our visual system cannot process the subtle chromatin features present in one nucleus compared to another over a hundred or several hundred nuclei. While all three have differing pathogenic mechanisms, this may be reflected in the nuclear morphology (size, chromatin patterns, etc.) that reflect the transcriptional and gene silencing activity for each lesion. For a given lesion, comparing nuclear morphology can allow the pathologist to distinguish or narrow the list of possibilities. This is particularly important in biopsy specimens where larger microarchitectural context is lost. The subcellular location of particular biomarkers may also help the pathologist distinguish between different pathologies.

In the case of the prostate, the research outcome would be to go beyond the current standard of Gleason scoring and provide a tool to select those patients who may have a low Gleason score but are likely to go on to have aggressive disease. Both nuclear morphology and location biomarkers may contribute to this distinction. In the case of the prostate, identifying patients at

high risk for aggressive disease is very relevant as this could prevent unnecessary and morbid therapy for the many men affected by prostate cancer.

The results of these translational studies are anticipated to improve patient outcomes through more appropriate choice of therapies and enhanced diagnostic capabilities. They will also set the stage for many additional studies for other tumor types using Omnyx' industry-leading digital pathology platform, enabling significant growth and job creation in Pennsylvania.

Summary of Research Completed

Aim 1. As described below, we have completed our development of both the location biomarkers and the morphology software, and have completed the liver study.

Improvement of algorithms for detecting Location Biomarkers
As reported last year, we have significantly improved the algorithms for identifying location biomarkers that were originally developed prior to this grant. The manuscript describing this work is being revised for resubmission. We have also added a new capability, which is to identify biochemical pathways that contain significant numbers of proteins that change location in cancer. These are listed in Table 1. It is important to note that the names of the pathways are based on the context in which they were originally described, and that they may play a role in more than one process. Identification of their potential involvement in cancer may help elucidate such roles.

Additional testing of algorithms for detecting morphology differences
While images were being collected, we sought to test the effectiveness of the transport-based image analysis pipeline developed in Dr. Rohde's laboratory using alternative datasets. We utilized already imaged data of Feulgen stained thyroid specimens to test whether the segmentation and nuclear morphometry pipeline could be used to effectively differentiate a variety of benign and malignant cancers using a large cohort of patients. During the course of this research, we experimented with several classification methods for single nuclei, in combination with voting strategies for sets of nuclei for a single patient. The results of this effort were recently published (Ozolek, et al., 2014) and are summarized in Table 2 below.

Preparation of slides for imaging and image collection
For the liver project, we obtained 186 terabytes of whole slide images, for 86 subjects and 15 antibodies plus traditional hematoxylin/eosin staining.

For the prostate project, we have not yet obtained images from Dr. Parwani's group. The slides are still being scanned and we will receive the images when they are collected.

Results from classification of liver images using location biomarkers
Four types of adult lesions were analyzed: Dysplastic nodules (DN, 13 cases), Focal nodular hyperplasia (FNH, 23 cases), Hepatocellular carcinoma (HCC, 16 cases), and Macroregenerative nodules (MRN, 14 cases). For beta-catenin, CRP, DEK, DKC, GS, HSP70, KI67, FABP, NDUFAF1, NPM1, and TJP, the accuracies for distinguishing the four classes all ranged

between 0.375 and 0.495 (for reference, an accuracy of 0.457 was obtained using Feulgen staining alone). Two proteins showed accuracies above 50%, IRX6 and Glypcan-3. The confusion matrices for them are shown below.

Antibody=IRX6; Accuracy = 0.55

True/pred	DN	FNH	HCC	MRN
DN	0.69	0.15	0.07	0.09
FNH	0.05	0.89	0.02	0.04
HCC	0.30	0.34	0.08	0.28
MRN	0.22	0.19	0.05	0.54

Antibody=Glypican-3; Accuracy = 0.62

True/pred	DN	FNH	HCC	MRN
DN	0.70	0.11	0.09	0.10
FNH	0.01	0.99	0.00	0.00
HCC	0.25	0.14	0.45	0.16
MRN	0.38	0.15	0.15	0.31

Three types of pediatric lesions were examined: Fetal hepatoblastoma (FHB, 6 cases), Hepatocellular adenoma (HCS, 4 cases), and Focal nodular hyperplasia (FNH, 3 cases). For CRP and L-FABP, accuracies ranged from 0.383-0.425. For beta-catenin, HSP70, IRX6, KI67, NDUFAF1, NPM1 and TJP!, accuracies ranged 0.513-0.63. These were all below the accuracy for Feulgen staining alone, 0.663. For DEK, DKC, GS, and Glypican-3, the accuracies were in the range of 0.675-0.717. The confusion matrices for the best two are shown below.

Antibody=DEK; Accuracy = 0.72

True/pred	DN	FNH	HCC
DN	0.56	0.33	0.11
FNH	0.18	0.70	0.13
HCC	0.06	0.05	0.89

Antibody=Glypican-3; Accuracy = 0.70

True/pred	DN	FNH	HCC
DN	0.80	0.10	0.10
FNH	0.29	0.39	0.33
HCC	0.03	0.05	0.93

Results from classification of liver images using morphology

Table 3 shows results obtained to date using the liver images obtained through this project. These were for 8 diagnostic challenges selected by Dr. JA Ozolek. They were selected due to their being common clinical decisions in current practice. For each diagnostic challenge, we report the average classification accuracy, as well as Cohen's kappa, a statistic meant to evaluate

how far the agreement is from chance (0 being pure chance, and 1 being complete agreement). With the exception of the Normal vs. Abnormal challenge, our preliminary results are good. A potential reason behind the poor results for Normal vs. Abnormal is that, the distribution of the data between normal and abnormal cases is unbalanced.

Aim 2. This aim was to develop appropriate interfaces to the technologies. Our work during the final year is described below.

Software for display of location biomarkers results to clinicians
Our location biomarkers software automatically selects regions from whole slide IHC images that are in focus and show antibody staining. These are used for classifying the sample as normal or abnormal. The issue then becomes how to communicate these results to the clinician. Recently, we have created an initial version of software for displaying the selected regions along a spectrum from most normal to most abnormal. Clicking on each image will display the region in the original whole slide image.

The idea behind this display is to first identify the primary "axis" in the feature space that differentiates normal regions from cancerous regions (for a given tissue). This is learned on training images for which the diagnosis is known. Features can then be calculated from regions of test images (regions from a patient image for which diagnosis is desired) and converted to a position along this axis. This allows all test regions to be displayed in order of their "normality." An example display using clustering is shown in Fig. 1. Because of the importance that we place on this project, we will complete development of this software with support from internal Carnegie Mellon sources.

Software for display of morphology results to clinicians
In (Ozolek, et al., 2014) we describe a method for visualizing the differences between two cell populations (e.g. benign vs. malignant). The method works by combining our previous work on penalized linear discriminant analysis (Wang, Mo, Ozolek , & Rohde, 2011), and linear optimal transport (Wang, Slepcev, Ozolek, Basu, & Rohde, 2013) (Basu, Kolouri, & Rohde, 2014). It modifies the approach presented earlier in (Wang, Slepcev, Ozolek, Basu, & Rohde, 2013) by selecting the regularization parameter of the penalized LDA technique we described in (Wang, Mo, Ozolek , & Rohde, 2011) by regression with an exponential function, as we described in (Basu, Kolouri, & Rohde, 2014). During experimentation with the thyroid H&E images we found this approach to be more robust with respect to our previous work. A representative result is shown in Fig. 2 below. The source code for this software is available at http://www.andrew.cmu.edu/user/gustavor/software.html. A graphical user interface allowing pathologists to utilize the software more seamlessly is the subject of current development, using internal funds.

Table 1. Pathways with significant location change but no significant expression change. Pathway p-values were calculated using individual protein p-values from the pipeline for the analysis set, and using p-values from gross pathologist annotations. For each type of p-value, those pathways whose p-value was lower than the Bonferroni-Holm threshold are marked (the threshold depends on the number of nodes in the pathway). These pathways show significant change in localization of their component proteins.

Pathway	Loc:Pipe	Exp:Pipe	Loc:Ann	Exp:Ann
Liver				
Chagas disease American trypanosomiasis	*		*	*
NOD like receptor signaling pathway	*		*	*
Long term depression	*			*
Valine, leucine and isoleucine degradation	*			*
Fatty acid elongation	*			*
Butanoate metabolism	*			
Thyroid cancer	*			
Prostate				
Amino sugar and nucleotide sugar metabolism	*			*
Histidine metabolism	*			

Table 2. Summary of classification performance comparisons between LOT and Feature based approaches.

Comparisons	**LOT**		**Feature**	
	Accuracy (%)	**Cohen's Kappa**	**Accuracy (%)**	**Cohen's Kappa**
FA vs. FC	100	1.00	87	0.74
FA vs. FVPC	100	1.00	97	0.93
FC vs. WIFC	100	1.00	76	0.45
FVPC vs. FC	87	0.67	90	0.78
FA vs. NG	100	1.00	84	0.67
FC vs. NG	100	1.00	81	0.60

Table 3– Classification results for liver dataset using morphology.

Comparisons	LOT	
	Accuracy (%)	Cohen's Kappa
Normal vs. Abnormal	60	0.01
Benign (MRN, FNH, HCA) vs. Malignant (DN, HCC)	82	0.63
(MRN, FNH) vs. HCA	90	0.65
DN vs. HCC	68	0.38
MRN vs. FNH	88	0.75
Normal vs. (FNH, MRN)	81	0.29
FHB vs. Normal (Kids only)	89	0.73
FHB vs. Normal (All)	92	0.83

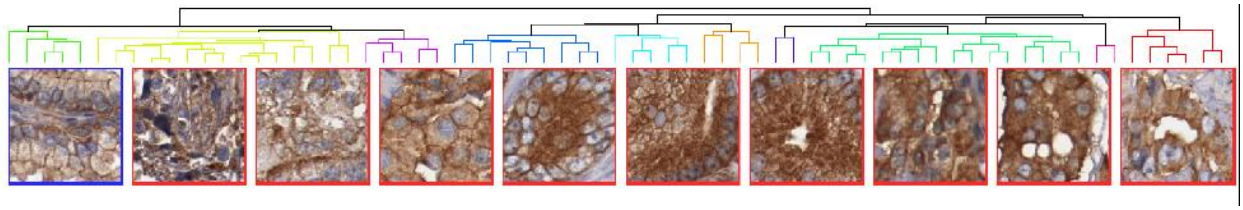

Figure 1. Ordering regions by location change progression. The regions of all images for a single protein are clustered into a binary hierarchical tree with optimal leaf ordering. The tree is cut at 10 clusters and leaves contained in each cluster are indicated by color. The region closest to the mean of each cluster is displayed below the tree. These results are for the protein TMOD3 in prostate. The image outlined in blue is from normal tissue, the tumor images are in red. Note that the images reveal progressive movement from the plasma membrane on the left (including the normal image) to a relatively homogenous cytoplasmic location.

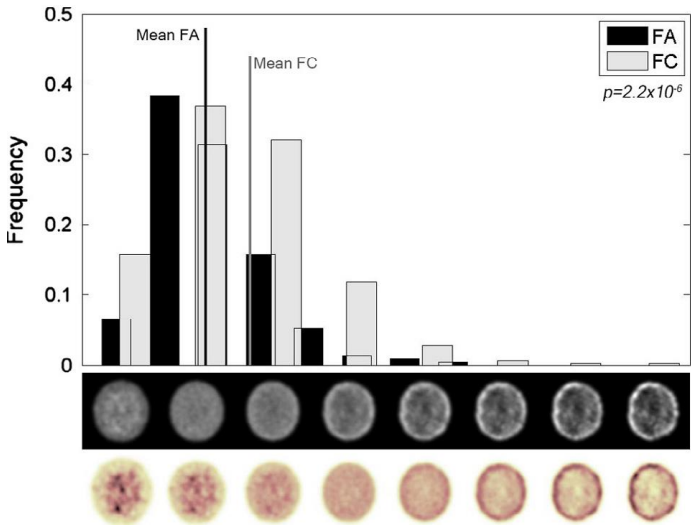

Figure 2 - Nuclei distribution histograms to distinguish between follicular adenoma (FA) and follicular carcinoma (FC). The rows of images of nuclei beneath the histogram bins are the normalized grayscale (upper) and colorized (lower) visual representations of nuclei along the optimal transportation pathway (geodesic) that best discriminates between FA and FC.

References

Basu, S., Kolouri, S., & Rohde, G. (2014). Detecting and visualizing cell phenotype differences from microscopy images using transport-based morphometry. *Proc Natl Acad Sci , 111*, 3448-3453.

Cheng , C., Wang , W., Ozolek, J., & Rohde, G. (2013). A flexible and robust approach for segmenting cell nuclei from 2D microscopy images using supervised learning and template matching. *Cytometry A , 83* (5), 495-507.

Ozolek, J., Tosun, A., Wang, W., Chen, C., Kolouri, S., Basu, S., et al. (2014). Accurate diagnosis of thyroid follicular lesions from nuclear morphology using supervised learning. *Medical Image Analysis , 18* (5), 772-780.

Wang, W., Mo, Y., Ozolek , J., & Rohde, G. (2011). Penalized Fisher discriminant analysis and its application to image-based morphometry. *Pattern Recognition Letters , 32* (15), 2128-2135.

Wang, W., Ozolek, J., & Rohde, G. (2010). Detection and classification of thyroid follicular lesions based on nuclear structure from histopathology images. *Cytometry Part A , 77* (5), 485-494.

Wang, W., Slepcev, D., Ozolek, J., Basu, S., & Rohde, G. (2013). A linear optimal transportation framework for quantifying and visualizing variations in sets of images. *Int J Comput Vision , 101*, 254-269.